Supporting Information

Enhanced activation of an amino-terminally truncated isoform of voltage-gated proton channel HVCN1 enriched in malignant B cells

Elayne Hondares, Mark Brown, Boris Musset, Deri Morgan, Vladimir V. Cherny, Christina Taubert, Mandeep K. Bhamrah, David Coe, Federica Marelli-Berg, John G. Gribben, Martin J.S. Dyer, Thomas E. DeCoursey, Melania Capasso

SUPPORTING FIGURES

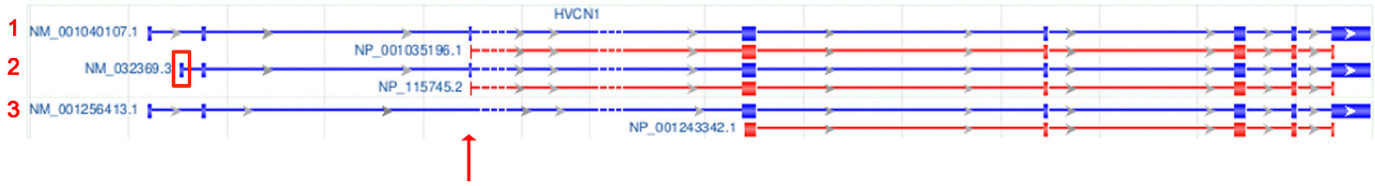

Fig. S1. Alignment of the 5′ regions of the three mRNA isoforms reported in the NCBI DNA and RNA database for human HVCN1. The blue lines represent mRNA and the red line protein (coding) sequences. The thicker regions indicate the exons, whereas the thinner regions correspond to the gene introns. We have included a red box to highlight the alternative 5′-UTR utilized by variant 2 and an arrow to indicate the missing exon in variant 3. Source: NCBI DNA and RNA database.

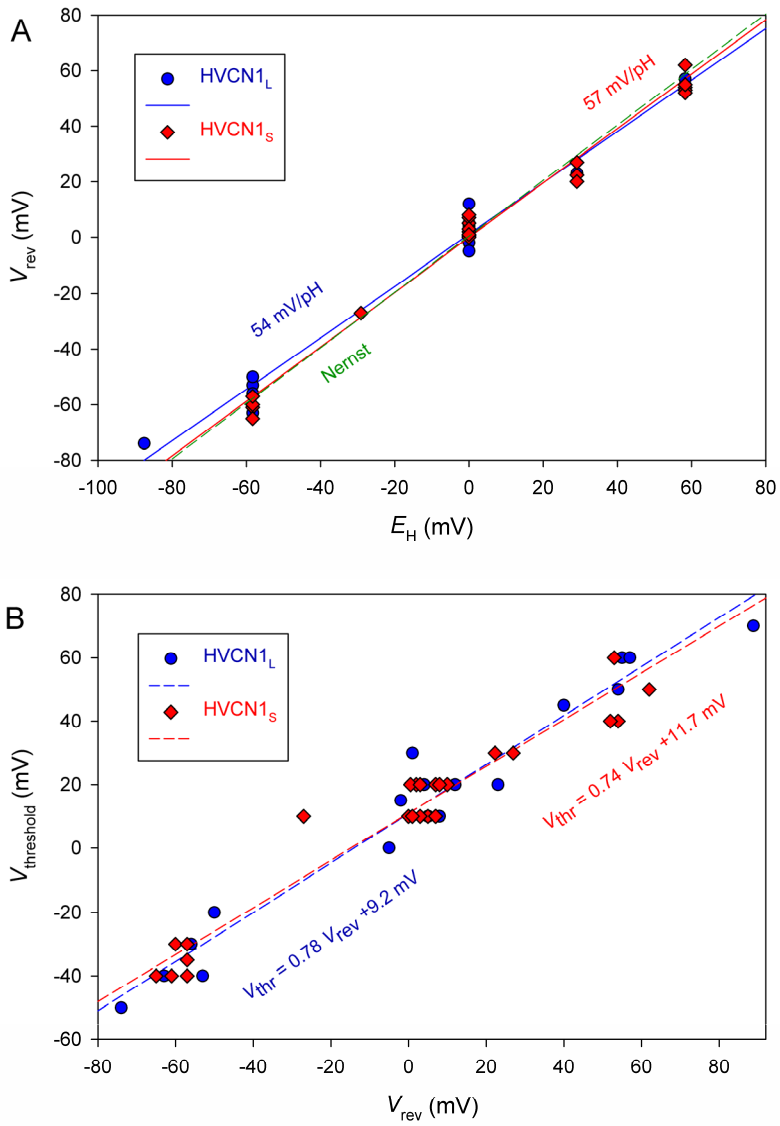

Fig. S2. A) Both HVCN1$_L$ (●) and HVCN1$_S$ (♦) are proton selective. In whole-cell configuration, V_{rev} was determined using tail currents. The range of pH_o studied was 4.6-8.0; the range of pH_i was 6.5-7.0. Lines show linear regression on each set, with slopes 52 mV (HVCN1$_L$) and 57.2 mV (HVCN1$_S$), compared with 58.2 mV calculated by the Nernst equation. B) The ΔpH dependence of gating of HVCN1$_L$ (●) and HVCN1S channels (♦) studied in whole-cell configuration is indistinguishable. The threshold voltage at which current is first activated, $V_{threshold}$, is plotted as a function of the measured V_{rev}. Dashed lines show linear regression on the data, with the equations provided. Identification of $V_{threshold}$ was based on the appearance of time dependent currents during test pulses, as well as the appearance of distinct tail currents upon repolarization.

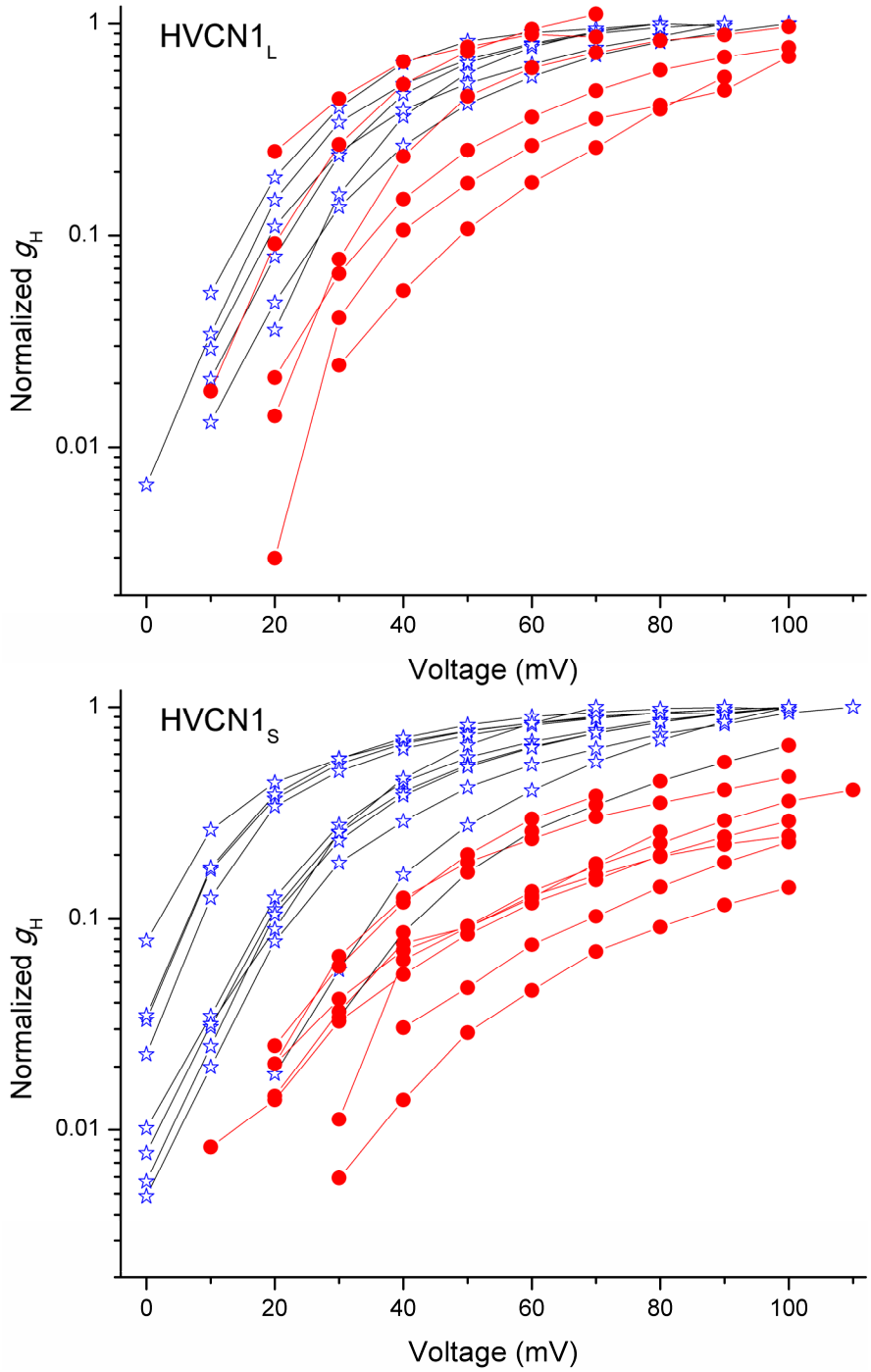

Fig. S3. HVCN1$_L$ responds to PMA stimulation, but HVCN1$_S$ responds more strongly. Plotted are g_H-V relationships in individual cells, connected by lines, normalized to the maximal value after PMA stimulation (blue stars). For each cell, the g_H-V relationship after GFX is also plotted (●). Although both isoforms respond, the increase in $g_{H,max}$ and the negative shift by PMA are both more profound in HVCN1$_S$.

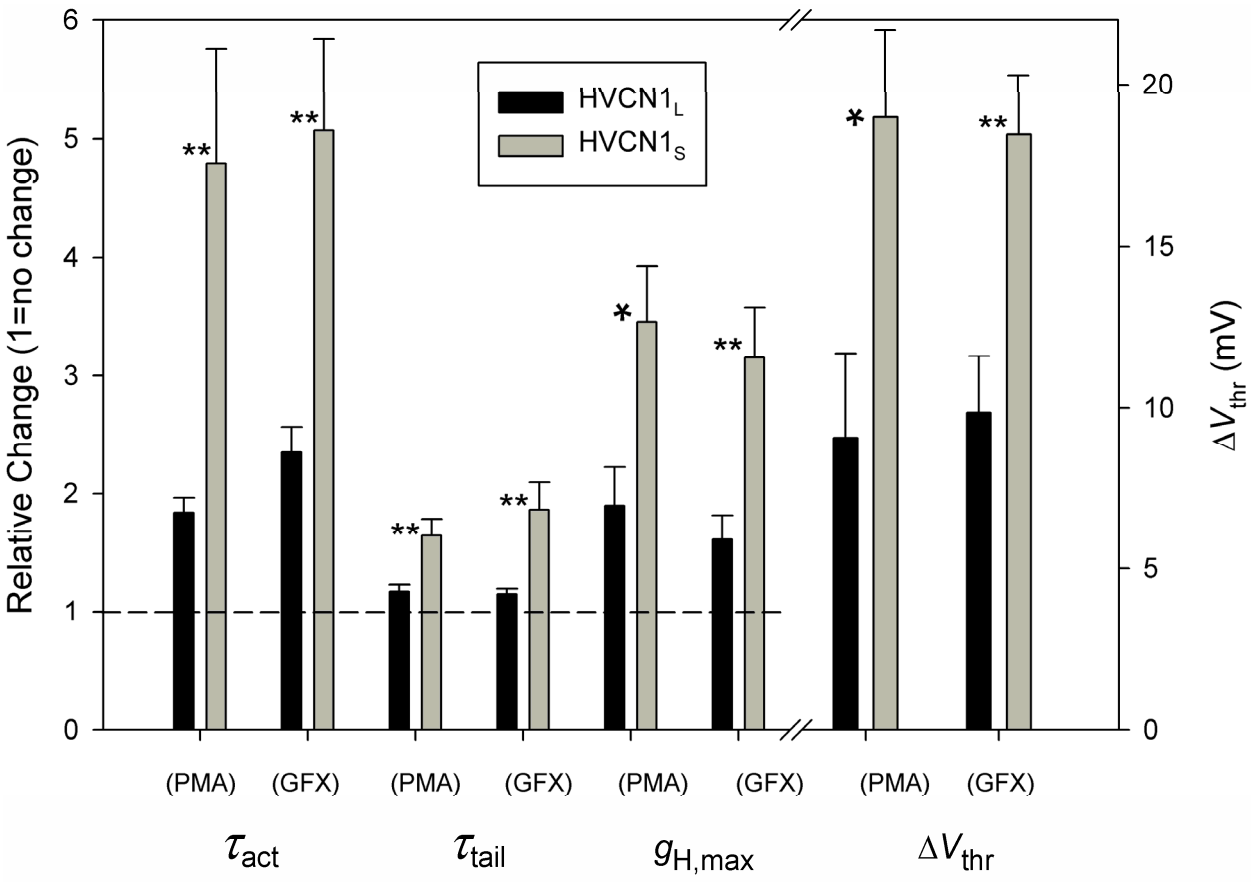

Fig. S4. The enhanced gating mode is more pronounced in $HVCN1_S$ (gray bars) than in $HVCN1_L$ (black). Mean ± SEM (n = 13-18 for $HVCN1_L$, 13-15 for $HVCN1_S$) changes produced in the four properties that differ in the enhanced gating mode are summarized. For each of the first three parameters, the relative change is plotted so that the effect increases relative to 1.0 (dashed reference line); the ratio for τ_{act} is (control/PMA), for τ_{tail} is (PMA/control), for $g_{H,max}$ is (control/PMA). Similarly, for GFX reversal, the ratio for τ_{act} is (GFX/PMA), for τ_{tail} is (PMA/GFX), for $g_{H,max}$ is (GFX/PMA). For the shift in $V_{threshold}$ the values show the absolute magnitude of the negative shift produced by PMA and the positive shift produced by GFX. For each parameter, the $HVCN1_S$ response is significantly greater than the $HVCN1_L$ response (*p<0.05, **p<0.01). For each parameter, the reversal by GFX is not significantly different from the effect of PMA.

In many human and mammalian cells, stimulation by agonists that act through activation of PKC results in strong amplification of the proton conductance (1-8), a phenomenon that has been called “enhanced gating.” Enhanced gating encompasses a predictable constellation of changes in the properties of proton channels (described in

this table); however, there are two subtypes of enhanced gating. In the full enhanced gating mode $V_{threshold}$ shifts by -30 to -40 mV, τ_{act} speeds typically 3-5-fold, τ_{tail} slows up to 3-5 fold, and $g_{H,max}$ increases by 2-4-fold. The full response occurs in cells with a high level of NADPH oxidase (NOX) activity; agents that activate NOX also produce enhanced gating of HVCN1 (9). Cells exhibiting a full response include human eosinophils (1, 2, 5, 10), neutrophils (3), monocytes (7), PLB-985 cells (11), and sperm (4), and mouse granulocytes (5), osteoclasts (6), and perhaps dendritic cells (12). A modified degree of enhanced gating occurs in cells lacking NOX activity; typically the g_H-V relationship shifts by -20 mV or less and τ_{tail} slows little or not at all (13). The PMA response observed here in cells expressing $HVCN1_S$ fits this pattern precisely, with a 5-fold speeding of τ_{act}, and a 3-fold increase in $g_{H,max}$, but τ_{tail} slowed less than 2-fold, and the g_H-V relationship shifted only -20 mV. Other cells that exhibit a partial response include human neutrophils from CGD patients lacking $gp91^{phox}$, PLB-985 cells with $gp91^{phox}$ knocked out (11), and human basophils (8). The PMA response observed here in $HVCN1_S$ is consistent with the low level of ROS production by LK35.2 cells.

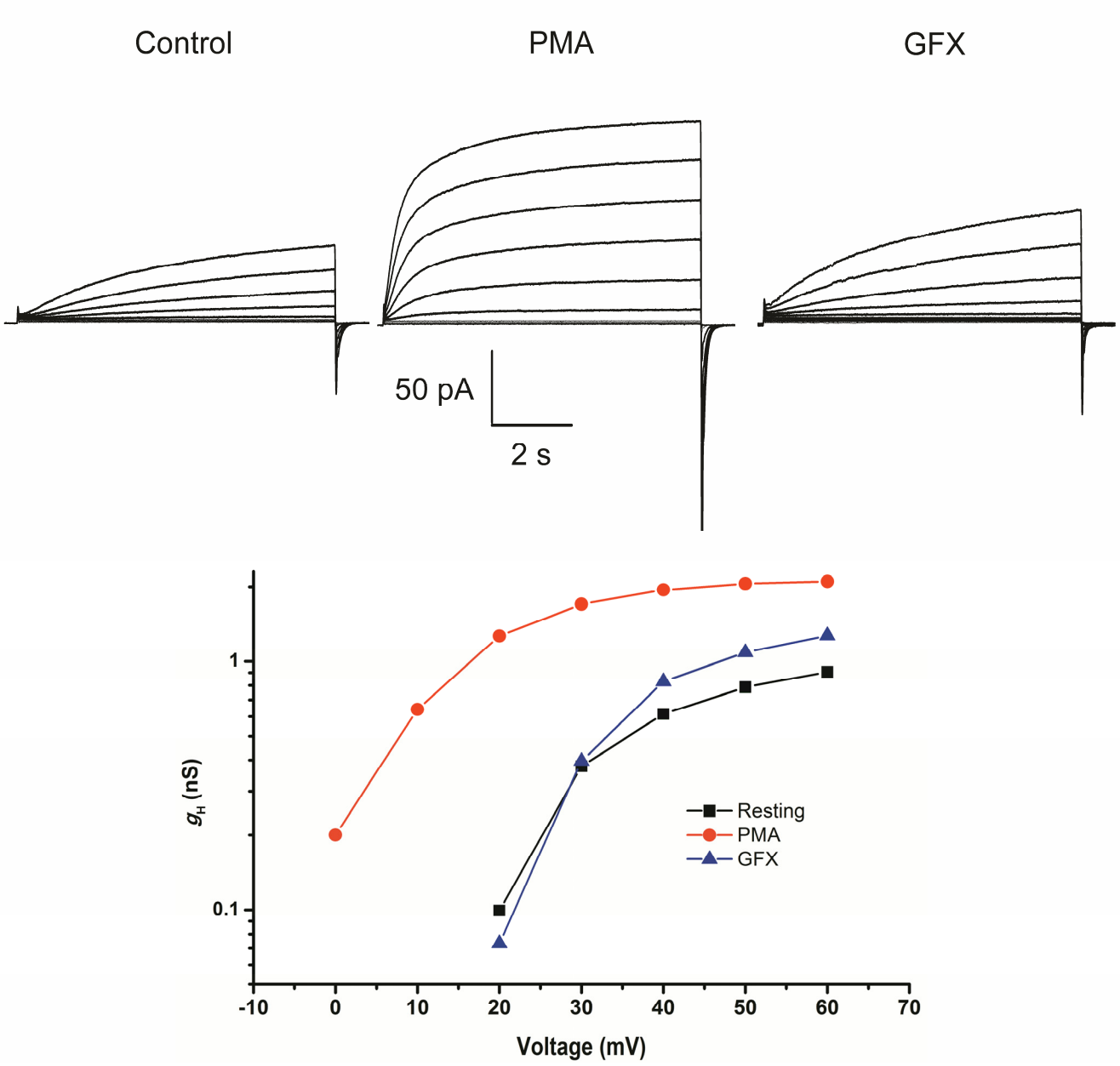

Fig. S5. Enhanced gating of proton channels in response to PMA and its reversal by GFX are illustrated in a B cell from a patient with CLL. Each family of currents was recorded during pulses from a holding potential of -40 mV in 10 mV increments up to 60 mV. The graph shows a large negative shift of the g_H-V relationship produced by PMA, and its complete reversal by GFX. Similar responses were observed in cells from three other patients. In 4 CLL cells (each from a different patient) τ_{act} was 4.0 ± 0.9 times faster and the mean $V_{threshold}$ shift was 18.8 ± 4.3 mV (mean ± SEM).

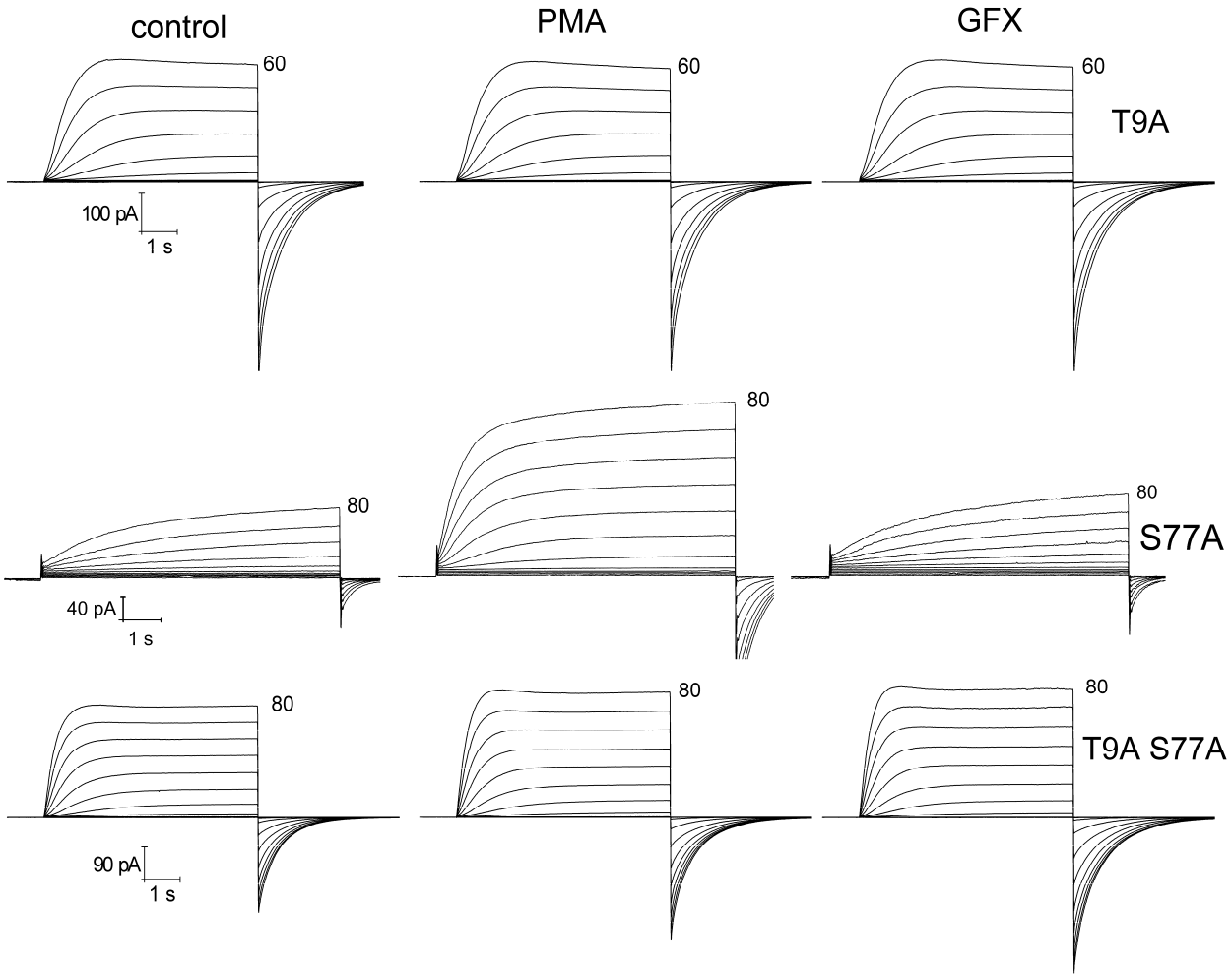

Fig. S6. The responses to PMA and GFX in three mutants of $HVCN1_S$. The T9A mutant of $HVCN1_S$ does not respond to PMA or GFX. The S77A mutant of $HVCN1_S$ responds distinctly to PMA and GFX, whereas the double mutant T9A/S77a also fails to respond. These results implicate Thr^9 as essential to the enhanced gating response. Families of currents in the same cell during identical voltage pulses before stimulation, after PMA, and after GFX treatment are shown for representative cells. Each cell was held at -40 mV and pulses were applied in 10 mV increments up to the indicated voltage. Note the rapid activation of cells with the T9A mutation (single or double).

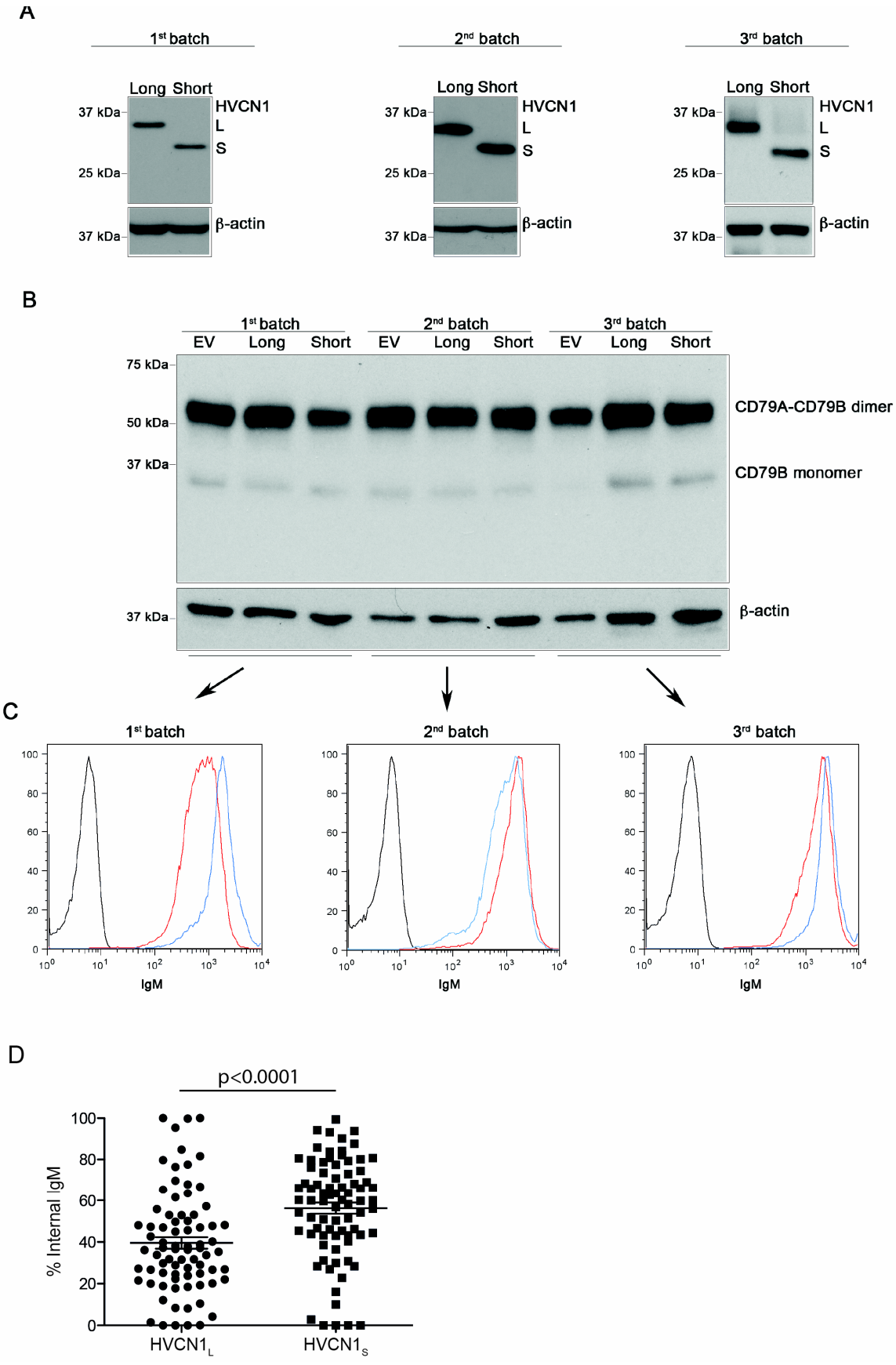
A
1st batch
2nd batch
3rd batch
Long Short
37 kDa
25 kDa
HVCN1
L
S
β-actin
B
1st batch
2nd batch
3rd batch
EV Long Short EV Long Short EV Long Short
75 kDa
50 kDa
37 kDa
CD79A-CD79B dimer
CD79B monomer
β-actin
C
1st batch
2nd batch
3rd batch
IgM
D
p<0.0001
% Internal IgM
HVCN1L
HVCN1S

Fig. S7. Levels of expression of HVCN1 and BCR complex components in A20 cell line overexpressing $HVCN1_L$ or $HVCN1_S$.

Three different batches of A20 cells were transduced with an empty vector (EV), $HVCN1_L$ (Long) or $HVCN1_S$ (Short). A) Immunoblot analysis showing $HVCN1_L$ (L) and $HVCN1_S$ (S) expression. β-actin was used as a loading control. B) Immunoblot of CD79B (immunoglobulin-associated-β or Ig-β), analyzed in non-reducing conditions. C) Flow cytometry analysis of IgM expression in the three different batches of cells. Blue histogram represents cells overexpressing $HVCN1_L$, red histogram cells overexpressing $HVCN1_S$ and black histogram unstained cells. D) Quantification of percentage of internalized IgM over total IgM in each cell. Each symbol represents a single cell (*n* = 78) and horizontal lines indicate the mean.

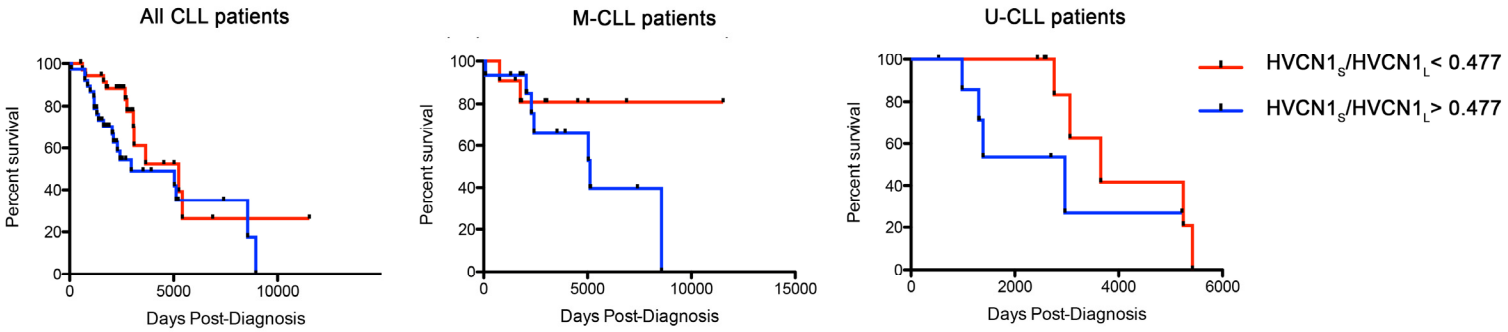

Fig. S8. CLL patients with higher expression of $HVCN1_S$ show a trend for reduced overall survival. *Left*) Kaplan-Meier curve for patients classified into either 'high' or 'low' for their ratio of $HVCN1_S$ expression over $HVCN1_L$ (red line = low $HVCN1_S$, blue line = high $HVCN1_S$), using the median ratio of 0.477 as a cut-off (Mantel-Cox $p = 0.0700$; red line $n = 36$, blue line $n = 38$). Levels of expression of $HVCN1_L$ and $HVCN1_S$ were determined by densitometry analysis of CLL protein lysates immunoblots, relative to loading control (α-tubulin) and normalized to a positive control used across different blots (cell line HBL1). (*Middle*) Kaplan-Meier curve for mutated (M-CLL) patients, classified as before ($p = 0.2747$; red line $n = 11$, blue line $n = 15$). (*Right*) Kaplan-Meier curve for unmutated (U-CLL) patients ($p = 0.1312$; red line $n = 10$, blue line $n = 7$).

Table S1. Gating kinetics of unstimulated LK35.2 cells with $HVCN1_S$, $HVCN1_L$, and $HVCN1_S$ mutants.

Construct	τ_{act} +60 mV (s)	τ_{tail} (ms)	$V_{threshold}$ (mV)
$HVCN1_S$	5.58 ± 1.13 (17)	370 ± 43 (19)	21.0 ± 2.2 (18)
$HVCN1_L$	* **2.24** ± 0.36 (10)	494 ± 88 (9)	15.6 ± 2.8 (11)
T9A	* **0.62** ± 0.076 (6)	453 ± 46 (8)	§ **-2.6** ± 3.6 (9)
S77A	3.91 ± 0.87 (8)	538 ± 83 (8)	* **12.0** ± 2.8 (8)
T9A/S77A	1.40 ± 0.82 (3)	399 ± 71 (5)	9.8 ± 6.5 (4)
T29A	‡ **0.51** ± 0.12 (5)	* **871** ± 59 (5)	§ **-12** ± 2.2 (5)
T29D	* **0.91** ± 0.44 (7)	508 ± 145 (8)	* **3.1** ± 3.5 (8)
S97A	2.14 ± 0.35 (6)	608 ± 79 (6)	19.5 ± 1.5 (6)
S97D	§ **0.77** ± 0.07 (25)	427 ± 53 (25)	12.6 ± 1.3 (25)
T29A/S97A	* **0.55** ± 0.11 (8)	* **848** ± 128 (8)	† **-3.8** ± 2.6 (8)

All cells were unstimulated and studied at pH_o = pH_i = 7.0 in perforated-patch configuration. Mean ± SEM (*n*) are given. Statistical differences from $HVCN1_S$ are indicated: * $p < 0.05$, ‡ $p < 0.01$, † $p < 0.001$, § $p < 0.0001$. The final five rows display data re-analyzed from a previous study of full–length HVCN1 expressed in LK35.2 cells (14). These values are compared statistically with $HVCN1_L$.

Table S2. Enhanced gating of $HVCN1_S$ with the S77A mutation in response to PMA or GFX.

S77A	τ_{act}		τ_{tail}		$g_{H,max}$		$V_{threshold}$	
	PMA	GFX	PMA	GFX	PMA	GFX	PMA	GFX
mean	2.34	3.20	1.31	1.26	1.86	2.38	14.0	7.5
SEM	0.47	0.89	0.12	0.16	0.25	0.66	2.4	2.5
n	6	4	6	4	6	4	5	4

Relative changes in each parameter are given (*i.e.*, 1.0 means no response). As in Fig. S5, the ratio for τ_{act} is (control/PMA), for τ_{tail} is (PMA/control), for $g_{H,max}$ is (control/PMA). For GFX reversal, the ratio for τ_{act} is (GFX/PMA), for τ_{tail} is (PMA/GFX), for $g_{H,max}$ is (GFX/PMA). $V_{threshold}$ values are the absolute magnitude of the negative shift produced by PMA and the positive shift produced by GFX. None of the responses differs significantly from $HVCN1_S$ responses, except for the GFX reversal of $V_{threshold}$, which was smaller for S77A.

Table S3. Characteristics of CLL Patients

			Clinical Data		Relative Expression of HVCN1				PKC	
Patient	Age	Sex	IGHV status	Survival (days)	$HVCN1_L$	$HVCN1_S$	Total	$HVCN1_S$/ $HVCN1_L$	Densitometry	+/-
B43	59	F		1632	2.9	1.6	4.5	0.5419	1.07994164	POS
B44	59	M		860	5	1.7	6.6	0.3376	0.929444745	POS
B45	88	F	M	85	2.9	1.3	4.2	0.4569	0.901620176	POS
B46	56	M		3073	5.5	3	8.5	0.5406	1.31332919	POS
B47	72	M	M	2953	2.5	0.9	3.4	0.3572	1.076176429	POS
B48	49	F		2807	5.6	3.2	8.8	0.5683	1.626910029	POS
B49	64	M		2710	5.5	2.7	8.2	0.4793	0.222747969	POS
B50	52	F		1160	15.7	12.8	28.6	0.8136	0.0754465	POS
B51	59	M		2527	3.5	2.1	5.6	0.6124	3.464993641	POS
B52	58	M		613	3.5	2.6	6	0.7521	0.506721317	POS
B53	66	F		8954	1.5	0.9	2.4	0.6174	0.153058909	POS
B54	75	F		2465	2.5	0.9	3.3	0.3421	0	NEG
B55	71	M		2345	2.2	3	5.2	1.3896	1.111757534	POS
B56	56	M		2437	1.3	1	2.3	0.7671	0	NEG
B57	80	F		2248	2.6	1.7	4.3	0.6659	2.631743971	POS
B58	56	M		3096	4.8	2.2	7	0.4585	0.082274197	POS
B59	82	M		1181	8.7	2.3	11	0.2689	0.972955833	POS
B60	87	M		726	3.6	1.6	5.2	0.4472	0.501670808	POS
B61	80	F		2248	8.7	3.5	12.2	0.4014	2.967775025	POS
B62	80	M	M	1758	3.9	1.4	5.3	0.3625	0.326367277	POS
B63	60	M		1788	9.3	2	11.3	0.2142	0.017556817	POS
B64	62	M		1706	15.8	3.3	19.1	0.2121	0.491560204	POS
B65	80	M		1858	10.5	5.4	15.8	0.5124	0.964239249	POS
B66	74	M		2673	6.9	1	7.9	0.1456	0.113335339	POS
B67	58	F		1553	19	3.8	22.9	0.2017	0	NEG
B68	82	M		1181	3.5	0.9	4.4	0.2499	1.474164936	POS
B69	74	M		2107	3.1	0.2	3.3	0.0628	0.59021759	POS
B70	83	M		1766	2.6	0.7	3.3	0.2613	1.086449383	POS
B71	60	M		2253	6.3	3	9.3	0.4761	0.308741844	POS
B72	54	M		1429	4.6	1.4	6	0.305	0.556051426	POS
B73	87	M		726	3.8	1.4	5.2	0.3566	1.945860305	POS
B74	79	M		2376	4.4	1.4	5.8	0.3204	0.089141168	POS
B75	63	F		2260	1	0.3	1.2	0.2651	1.496196771	POS
B76	59	F		1632	9	4.5	13.5	0.5046	1.936510285	POS
L1	68	m	U	2757	12.3	4	16.2	0.3222	0.48418262	POS
L10	52	m	U	2568	15.6	6.8	22.5	0.4375	0.016663283	POS
L11	65	m	M		24.4	14	38.4	0.5757	0	NEG
L12	66	m	U	1389	18.1	10.7	28.8	0.5904	0.460398151	POS
L13	76	f	U	2434	16.7	0.7	17.4	0.0389	0	NEG

L14	78	f	M	2042	4.8	1.7	6.5	0.3615	0.849684093	POS
L15	52	m	U	5219	15.8	5.7	21.5	0.3574	0.807601688	POS
L16	59	m	M	7403	3.6	0.7	4.3	0.2083	0.902562487	POS
L17	58	m	U	1315	8.8	5.9	14.8	0.6697	1.335926487	POS
L18	60	f	M	1299	15	11.2	26.3	0.7448	0	NEG
L19	84	f	U	984	5.6	0.8	6.3	0.1388	0	NEG
L2	62	f	M	2296	17.7	10.9	28.6	0.6162	0	NEG
L20	53	m	U	5420	137.8	77.4	164.1	0.5613	1.301714473	POS
L21	68	f	M	3917	40.4	19.1	45.4	0.4734	0	NEG
L22	76	m	M	2418	11.6	13.5	19.2	1.1663	0.153943666	POS
L23	61	m	M	2068	26.9	30.4	43.7	1.1291	0.210359159	POS
L24	78	f	M	1819	144.6	39	140	0.2693	0.035721496	POS
L25	59	m	U	5246	25.9	20.4	35.3	0.7874	0.346232682	POS
L26	65	m	M	1777	79.2	49.5	98.1	0.6248	0.264791187	POS
L27		f	U		9.6	5.9	15.5	0.6207	0.223836649	POS
L28	52	m	M	11525	4.6	1.8	6.4	0.3926	0.195476388	POS
L29	57	f	M	6883	5.6	3.3	8.9	0.5879	0.411740779	POS
L3	78	m	U	1305	9.3	6.2	15.5	0.6674	0.094403426	POS
L30	60	f	U	2603	6.7	4.9	11.6	0.7283	1.720449536	POS
L31	62	m	M	5148	4.4	2.6	7	0.5815	0.945405162	POS
L32	56	m	M	1518	6.3	2.5	8.9	0.4018	0.783520755	POS
L33	47	m	U	3060	4.5	1.8	6.2	0.394	0.821684589	POS
L34	76	m	M	3037	3.3	2.9	6.2	0.8745	0.335089518	POS
L35	58	m	M	4526	5.5	2.6	8.1	0.4739	0.252284566	POS
L36	54	m	U	532	6.6	5.3	11.9	0.8019	0.054676042	POS
L37	55	f	M	5022	6.4	4.6	11	0.7261	0.322348723	POS
L38	68	m	M	1760	2.3	4.5	6.8	1.9503	0.791368449	POS
L39	80	m	M	763	12	9.1	21.1	0.7548	0.768639263	POS
L4	62	f	U	2966	5.1	1.8	6.9	0.3455	0.612410555	POS
L40	59	m	U	3656	81	39.1	120.1	0.4824	0	NEG
L41	77	f	U	2757	10.6	8.8	19.5	0.8304	0.149925269	POS
L42	56	m	U	2694	27.1	19.8	46.9	0.7293	0.583203639	POS
L5	76	m	M	5038	4.6	1.5	6.1	0.318	0.017601259	POS
L6	58	m	M	1896	10	2.1	12	0.2095	0.088580175	POS
L7	66	f	M	8566	4.2	1.3	5.5	0.3075	0.212741553	POS
L8	52	f	M	5119	3.5	2.2	5.7	0.6417	0.468254735	POS
L9	64	m	M	3527	22	10.9	33	0.4951	0	NEG

IGHV status: mutation status of the immunoglobulin variable heavy chain variable region at the time of sampling; either mutated (M) or unmutated (U). Survival: time in days between diagnosis and death or database last update.

HVCN1 and PKC protein expression levels as determined by western blot, relative to loading control (α-tubulin) and normalized to positive control (HBL1 lysate). PKC expression considered positive (Pos) if greater than 0 or negative (Neg) if equal to 0. Samples were collected from patients evaluated at St Bartholomew's (London) and Leicester Royal Infirmary hospitals after they provided written informed consent, in accordance with the Declaration of Helsinki.

Supporting Materials and Methods

Gradient PCR

HBL1 cells were lysed using QIAshredder spin columns (Qiagen; 79656), total RNA extracted using RNeasy Mini Kit (Qiagen; 74106) and genomic DNA degraded with RNase-free DNase Set (Qiagen; 79254). cDNA was then synthesized using High Capacity cDNA Reverse Transcription Kit (Applied Biosystems; 4368814) all according to the manufacturer's instructions.

Gradient PCR reactions with annealing temperatures ranging from 49-72°C were carried out for 35 cycles on a Tetrad PTC-225 Thermal Cycler (MJ Research).

Pfx50™ DNA Polymerase (Invitrogen; 12355-012) was used according to manufacturers instructions with 0.3 mM dNTPs (Qiagen; 201913) and 2 μl of cDNA template. The reverse primer used for all pairs was 5′-CTCAACATGCCCCTGAAGTC-3′. The forward primer to recognize all 3 variants: 5′-CGCTGAGAGGATGAGCAAGT-3′; variant 2: 5′-TGCTCTGAGGCTCCCAGT-3′; variants 1 and 3: 5′-GTACGAGTTGGCCCGGAG-3′. All primers synthesized by Sigma Aldrich.

Reaction products were run on 2% agarose gels supplemented with 10% GelRed Nucleic Acid Gel Stain (Biotium; 41003) and HyperLadder IV (Bioline; BIO-33056) for DNA molecular weight markers.

Retroviral production and cell transduction

Retroviral particles were produced in Phoenix α packaging cells. Cells were transfected with MigRI empty vector and HVCN1 constructs (See materials & methods) by Ca^{2+} phosphate. Viral supernatants were collected after 24, 36 and 48 h.

A20 D1.3 and LK35.2 HyHEL10 cell lines were transduced by spinoculation at 2300 rpm for 90 min in the presence of 4 μg/ml Polybrene (Sigma Aldrich), three times over a period of 2 days.

Co-Immunoprecipitation assay

A20 D1.3 cells overexpressing $HVCN1_L$ or $HVCN1_S$ were lysed for 30 min in 20 mM Hepes, 1% CHAPS (3-[(3-Cholamidopropyl)-dimethylammonio]-1-propanesulfonate hydrate), 137 mM NaCl, 2 mM EDTA and proteases inhibitors (Sigma Aldrich). After

centrifuging the lysate at 12,000g for 10 minutes to sediment cell debris, supernatants were cleared with Protein G Sepharose beads (GE Healthcare). Immunoprecipitation was carried out using 1 mg anti-myc tag antibody (9B11; Cell Signaling Technology), or anti-CD79B (or immunoglobulin-associated-β; AT107-2; Serotec) conjugated to Protein G Sepharose beads. An equal amount of Protein-G beads conjugated to mouse or rat IgG were used as negative control. After washing with lysis buffer, beads were resuspended in 2x Laemmli sample buffer without β-mercaptoethanol (non-reducing conditions) and analyzed by western blot.

Immunofluorescence Microscopy

A20 D1.3 cells were stimulated with APC-conjugated $F(ab')_2$ anti-IgM (Jackson Laboratories) at 37°C for 30 min, washed with PBS and added to poly-L-lysine coated glass slides. Cells were then fixed in 4% paraformaldehyde for 20 min, washed three times with 0.1% saponin in PBS and blocked with 5% goat serum, 0.1% saponin in PBS for 10 min before being incubated overnight at 4°C in a humid chamber with AlexaFluor555-conjugated anti-myc (Cell Signaling; 9B11) in PBS with 5% goat serum and 0.1% saponin. Cells were subsequently washed twice, incubated with DAPI for 5 min, washed a final time and mounted with glass coverslips with ProLong® Gold Antifade Mountant (Life Technologies; P36930).

Slides were visualized using the Zeiss LSM 510 Meta Confocal Microscope.

Western Blot

Cell samples were lysed in SDS sample buffer (0.5M Tris-HCl pH 6.8, 20% glycerol, 4% SDS, 2% β-mercaptoethanol, ddH_2O and bromphenol blue) and sonicated for 10 s pulses, three times.

Proteins were separated by electrophoresis in 10% Mini-PROTEAN® TGX™ Gels (BioRad; 456-1034) at 90V and subsequently transferred to PVDF membranes (Perkin Elmer) by wet transfer.

Membranes were blocked with 5% Milk Powder in PBS for 45 min then incubated with either rabbit anti-HVCN1 (CovalAb), rabbit anti-phospho-PKC (pan) (Cell Signaling; 9371S), rabbit anti-phospho-p44/42 MAPK (Erk) (Cell Signaling; D13.14.4E), mouse

anti-p44/42 MAPK (Cell Signaling; 4696), mouse anti-β-actin (Cell Signaling; 4970) or mouse anti-α-tubulin (eBiosciences; 14-4502-82), either overnight at 4°C or 1 h at room temperature. Membranes were subsequently washed three times with PBST (0.05%TWEEN in PBS) before incubation for 1 h at room temperature with either HRP-conjugated anti-rabbit or –mouse (GE Healthcare; NA9340V – NXA931), as appropriate. Finally, they were washed a further three times with PBST before being covered with the chemiluminescence agent, ECL (GE Healthcare; RPN2106) and exposed to X-ray film (Fuji Film; 4741019236).
Densitometry was performed using ImageJ 1.45s software.

Migration assay

$3x10^5$ A20 D1.3 overexpressing EV, $HVCN1_L$ or $HVCN1_S$ were seeded onto transwell inserts with 5 μm pore size polycarbonate membranes (Corning), and either media or media containing 100ng/ml CXCL12 was added in the bottom of the well. Cells migrated into the well were re-suspended and their number determined by counting on a haemocytometer after 4h.

Proliferation assay

Cell proliferation was determined using the Click-iT Edu Imaging Kit (Invitrogen), according to the manufacturer's instructions. $5x10^5$ cells were incubated with 5 μM 5-ethynyl-2'-deoxyuridine (Edu) for 3h at 37°C. Subsequently, cells were fixed with 3.7 % formaldehyde for 15 min and permeabilized with 0.5 % Triton X-100 for 20 min. Immunofluorescent staining was carried out by incubation with anti-GFP, chicken IgY antibody (Invitrogen; A10262) for 1h. After two washes, cells were incubated with the Click-iT reaction cocktail for 30 minutes, in the dark. Finally, cells were incubated with Alexa Fluor 488 goat anti-chicken antibody (Invitrogen; A11039) for 40 minutes. Nuclei were stained with DAPI, and cells mounted with glass coverslips with ProLong® Gold Antifade mounting solution (Life Technologies). Cells were visualized using Zeiss LSM 510 Meta Confocal Microscope.

Supporting Information References

1. Bánfi B, et al. (1999) A novel H^+ conductance in eosinophils: unique characteristics and absence in chronic granulomatous disease. *J Exp Med* 190(2):183-94.
2. DeCoursey TE, Cherny VV, DeCoursey AG, Xu W, Thomas LL (2001) Interactions between NADPH oxidase-related proton and electron currents in human eosinophils. *J Physiol* 535(Pt 3):767-81.
3. DeCoursey TE, Cherny VV, Zhou W, Thomas LL (2000) Simultaneous activation of NADPH oxidase-related proton and electron currents in human neutrophils. *Proc Natl Acad Sci USA* 97(12):6885-9.
4. Lishko PV, Botchkina IL, Fedorenko A, Kirichok Y (2010) Acid extrusion from human spermatozoa is mediated by flagellar voltage-gated proton channel. *Cell* 140(3):327-337.
5. Morgan D, et al. (2007) Sustained activation of proton channels and NADPH oxidase in human eosinophils and murine granulocytes requires PKC but not $cPLA_2\alpha$ activity. *J Physiol* 579(Pt 2):327-44.
6. Mori H, et al. (2003) Regulatory mechanisms and physiological relevance of a voltage-gated H^+ channel in murine osteoclasts: phorbol myristate acetate induces cell acidosis and the channel activation. *J Bone Miner Res* 18(11):2069-76.
7. Musset B, Cherny VV, DeCoursey TE (2012) Strong glucose dependence of electron current in human monocytes. *Am J Physiol Cell Physiol* 302:C286-C295.
8. Musset B, et al. (2008) A pH-stabilizing role of voltage-gated proton channels in IgE-mediated activation of human basophils. *Proc Natl Acad Sci USA* 105(31):11020-11025.
9. DeCoursey TE (2010) Voltage-gated proton channels find their dream job managing the respiratory burst in phagocytes. *Physiology (Bethesda)* 25(1):27-40.
10. Cherny VV, Henderson LM, Xu W, Thomas LL, DeCoursey TE (2001) Activation of NADPH oxidase-related proton and electron currents in human eosinophils by arachidonic acid. *J Physiol* 535(Pt 3):783-94.
11. DeCoursey TE, Cherny VV, Morgan D, Katz BZ, Dinauer MC (2001) The $gp91^{phox}$ component of NADPH oxidase is not the voltage-gated proton channel in phagocytes, but it helps. *J Biol Chem* 276(39):36063-6.
12. Szteyn K, Yang W, Schmid E, Lang F, Shumilina E (2012) Lipopolysaccharide-sensitive H^+ current in dendritic cells. *Am J Physiol Cell Physiol* 303(2):C204-12.
13. Musset B, Cherny VV, Morgan D, DeCoursey TE (2009) The intimate and mysterious relationship between proton channels and NADPH oxidase. *FEBS Lett* 583(1):7-12.
14. Musset B, et al. (2010) Identification of Thr^{29} as a critical phosphorylation site that activates the human proton channel *Hvcn1* in leukocytes. *J Biol Chem* 285(8):5117-21.